 CMES, vol.12, no.1, pp.67-81, 2006

Past Cone Dynamics and Backward Group Preserving Schemes for Backward Heat Conduction Problems

C.-S. Liu [1], **C.-W. Chang** [2], **J.-R. Chang** [2]

Abstract: In this paper we are concerned with the backward problems governed by differential equations. It is a first time that we can construct a backward time dynamics on the past cone, such that an augmented dynamical system of the Lie type $\dot{\mathbf{X}} = \mathbf{B}(\mathbf{X},t)\mathbf{X}$ with $t \in \mathbb{R}^-$, $\mathbf{X} \in \mathbb{M}^{n+1}$ lying on the past cone and $\mathbf{B} \in so(n,1)$, was derived for the backward differential equations system $\dot{\mathbf{x}} = \mathbf{f}(\mathbf{x},t)$, $t \in \mathbb{R}^-, \mathbf{x} \in \mathbb{R}^n$. These two differential equations systems are mathematically equivalent. Then we apply the backward group preserving scheme (BGPS), which is an explicit single-step algorithm formulated by an exponential mapping to preserve the group preperties of $SO_o(n,1)$, on the backward heat conduction problem (BHCP). It can retrieve all the initial data with high order accuracy. Several numerical examples of the BHCP were work out, and we show that the BGPS is applicable to the BHCP, even those of strongly ill-posed ones. Under the noisy final data the BGPS is also robust to against the disturbance. The one-step BGPS effectively reconstructs the initial data from a given final data, with a suitable grid length resulting into a high accuracy never seen before. The results are very significant in the computations of BHCP.

keyword: Past cone dynamics, Backward group preserving scheme, Backward heat conduction problem, Strongly ill-posed problem.

1 Introduction

Time has two directions: past and future. The time dynamics that goes to future is known as a forward problem, and that goes to past is called a backward problem. For the forward problem which governed by ordinary differential equations (ODEs), Liu (2001) has derived a Lie group transformation for the augmented dynamics on the future cone, and developed group preserving scheme for an effective numerical calculation of nonlinear differential equations. Recently, the group preserving scheme is also proved to be very effective to deal with ODEs with special structures as shown by Liu (2005a) for stiff equations and by Liu (2005b) for ODEs with constraints.

Group-preserving scheme (GPS) can preserve the internal symmetry group of the considered system. Although we do not know previously the symmetry group of nonlinear differential equations systems, Liu (2001) has embedded them into the augmented dynamical systems, which concern with not only the evolution of state variables but also the evolution of the magnitude of state variables vector. That is, for an n ODEs system:

$$\dot{\mathbf{x}} = \mathbf{f}(\mathbf{x},t), \quad \mathbf{x} \in \mathbb{R}^n, \quad t \in \mathbb{R}^+, \tag{1}$$

we can embed it to the following $n+1$-dimensional augemented dynamical system:

$$\frac{d}{dt}\begin{bmatrix} \mathbf{x} \\ \|\mathbf{x}\| \end{bmatrix} = \begin{bmatrix} \mathbf{0}_{n\times n} & \frac{\mathbf{f}(\mathbf{x},t)}{\|\mathbf{x}\|} \\ \frac{\mathbf{f}^T(\mathbf{x},t)}{\|\mathbf{x}\|} & 0 \end{bmatrix} \begin{bmatrix} \mathbf{x} \\ \|\mathbf{x}\| \end{bmatrix}. \tag{2}$$

Here we assume $\|\mathbf{x}\| > 0$ and hence the above system is well-defined.

It is obvious that the first row in Eq. (2) is the same as the original equation (1), but the inclusion of the second row in Eq. (2) gives us a Minkowskian structure of the augmented state variables of $\mathbf{X} := (\mathbf{x}^T, \|\mathbf{x}\|)^T$ satisfying the cone condition as shown in Fig. 1:

$$\mathbf{X}^T\mathbf{g}\mathbf{X} = 0, \tag{3}$$

where

$$\mathbf{g} = \begin{bmatrix} \mathbf{I}_n & \mathbf{0}_{n\times 1} \\ \mathbf{0}_{1\times n} & -1 \end{bmatrix} \tag{4}$$

is a Minkowski metric, $\mathbf{I}_n$ is the identity matrix of order n, and the superscript T stands for the transpose. In terms of $(\mathbf{x}, \|\mathbf{x}\|)$, Eq. (3) becomes

$$\mathbf{X}^T\mathbf{g}\mathbf{X} = \mathbf{x}\cdot\mathbf{x} - \|\mathbf{x}\|^2 = \|\mathbf{x}\|^2 - \|\mathbf{x}\|^2 = 0, \tag{5}$$

[1] Corresponding author. E-mail: csliu@mail.ntou.edu.tw, Department of Mechanical and Mechatronic Engineering, Taiwan Ocean University, Keelung, Taiwan

[2] Department of Systems Engineering and Naval Architecture, Taiwan Ocean University, Keelung, Taiwan

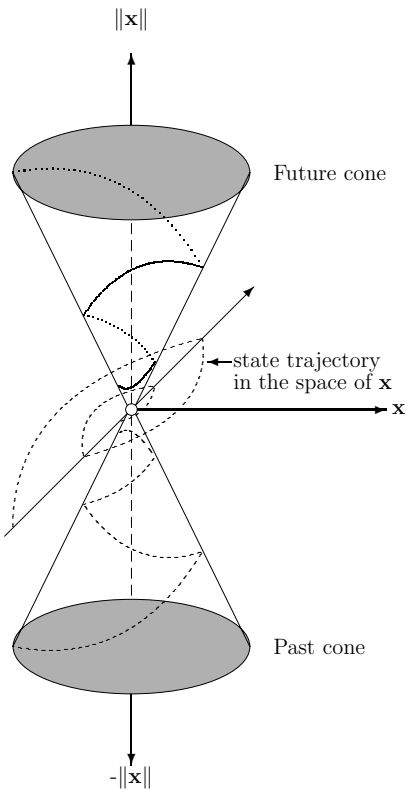

Figure 1 : The construction of deleted cones in the Minkowski space for forward and backward problems signifies a conceptual breakthrough. The trajectory observed in the state space **x** is a parallel projection of the trajectory in the null cones along the $\|\mathbf{x}\|$ or $-\|\mathbf{x}\|$-axis.

where the dot between two n-dimensional vectors denotes their Euclidean inner product. The cone condition is thus the most natural constraint that we can impose on the dynamical system (2).

Consequently, we have an $n+1$-dimensional augmented system:

$$\dot{\mathbf{X}} = \mathbf{A}\mathbf{X} \tag{6}$$

with a constraint (3), where

$$\mathbf{A} := \begin{bmatrix} \mathbf{0}_{n\times n} & \frac{\mathbf{f}(\mathbf{x},t)}{\|\mathbf{x}\|} \\ \frac{\mathbf{f}^T(\mathbf{x},t)}{\|\mathbf{x}\|} & 0 \end{bmatrix}, \tag{7}$$

satisfying

$$\mathbf{A}^T\mathbf{g} + \mathbf{g}\mathbf{A} = \mathbf{0}, \tag{8}$$

is a Lie algebra $so(n,1)$ of the proper orthochronous Lorentz group $SO_o(n,1)$. This fact prompts us to devise the so-called group-preserving scheme, whose discretized mapping **G** exactly preserves the following properties:

$$\mathbf{G}^T\mathbf{g}\mathbf{G} = \mathbf{g}, \tag{9}$$

$$\det \mathbf{G} = 1, \tag{10}$$

$$G_0^0 > 0, \tag{11}$$

where G_0^0 is the 00th component of **G**. Such **G** is a proper orthochronous Lorentz group denoted by $SO_o(n,1)$.

Remarkably, the original n-dimensional dynamical system (1) in $\mathbb{E}^n$ can be embedded naturally into an augmented $n+1$-dimensional dynamical system (6) in $\mathbb{M}^{n+1}$. That two systems are mathematically equivalent. Although the dimension of the new system is raising one more, it has been shown that under the Lipschitz condition of

$$\|\mathbf{f}(\mathbf{x},t) - \mathbf{f}(\mathbf{y},t)\| \le \mathcal{L}\|\mathbf{x}-\mathbf{y}\|, \ \ \forall\, (\mathbf{x},t),(\mathbf{y},t) \in \mathbb{D}, \tag{12}$$

where $\mathbb{D}$ is a domain of $\mathbb{R}^n \times \mathbb{R}$, and $\mathcal{L}$ is known as a Lipschitz constant, the new system has the advantage of devising group-preserving numerical scheme as follows [Liu (2001)]:

$$\mathbf{X}_{\ell+1} = \mathbf{G}(\ell)\mathbf{X}_\ell, \tag{13}$$

where $\mathbf{X}_\ell$ denotes the numerical value of **X** at the discrete time t_ℓ, and $\mathbf{G}(\ell) \in SO_o(n,1)$ is the group value at time t_ℓ.

In this paper we attempt to develop group-preserving scheme for backward problems. It is an extension of the work by Liu (2004) by taking the time backward of equations into account on the construction of backward group theory. Numerical schemes adopted for backward problems are usually implicit. The explicit schemes that have been applied to solving the backward problems are apparently not very effective up to now. As mentioned by Mera (2005) the backward problem is ill-posed that is impossible to solve using classical numerical methods and requires special techniques to be employed.

The new method would provide us an explicit single-step algorithm, and renders a more compendious numerical implementation than other schemes to solve backward problems. The main motivation is placed on an

effective numerical solution of the backward heat conduction problem (BHCP). The BHCP is one of the inverse problem, which is different from the sideways heat conduction problem recently reviewed and calculated by Chang, Liu and Chang (2005) with the GPS method. The degree of the ill-posedness of BHCP is over other inverse heat conduction problems including the the sideways heat conduction problem, which is dealed with the reconstruction of unknown boundary conditions.

The BHCP is an ill-posed problem in the sense that the solution is unstable for a given final data $u_{\rm F}$. For example, $u(x,t)=\exp[\alpha^2(T-t)]\sin\alpha x$ is the solution of

$$\frac{\partial u}{\partial t}=\frac{\partial^2 u}{\partial x^2}, \tag{14}$$

subjecting to the final data $u(x,T)=\sin\alpha x$. Thus, by taking α arbitrarily large $u(x,0)=\exp[\alpha^2 T]\sin\alpha x$ can become unbounded.

In order to calculate the BHCP, there appears certain progress in this issue, including the boundary element method [Han, Ingham and Yuan (1995)], the iterative boundary element method [Mera, Elliott, Ingham and Lesnic (2001); Mera, Elliott and Ingham (2002)], the regularization technique [Muniz, de Campos Velho and Ramos (1999); Muniz, Ramos and de Campos Velho (2000)], the operator-splitting method [Kirkup and Wadsworth (2002)], the lattice-free high-order finite difference method [Iijima (2004)], and the contraction group technique [Liu (2004)]. A recent review of the numerical BHCP was provided by Chiwiacowsky and de Campos Velho (2003).

Through our study in this paper, it would be clear that the new method greatly reduces the computational time and is very easy to implement on the calculation of backward problems, including the BHCP as special case. This is an important contribution for calculating the backward problems.

2 GPS for differential equations system

2.1 The Cayley transform

The Lie group generated from $\mathbf{A}\in so(n,1)$ is known as a proper orthochronous Lorentz group. One of which is the Cayley transform

$$\mathrm{Cay}(\tau\mathbf{A})=(\mathbf{I}_{n+1}-\tau\mathbf{A})^{-1}(\mathbf{I}_{n+1}+\tau\mathbf{A}), \tag{15}$$

a mapping from $\mathbf{A}$ to an element of $SO_o(n,1)$ for $\tau\in\mathbb{R}$ and $\tau^2<\|\mathbf{x}\|^2/\|\mathbf{f}\|^2$. Substituting Eq. (7) for $\mathbf{A}(\ell)$, which denotes the value of $\mathbf{A}$ at the discrete time t_ℓ, into the above equation yields

$$\mathrm{Cay}[\tau\mathbf{A}(\ell)]=\begin{bmatrix}\mathbf{I}_n+\frac{2\tau^2}{\|\mathbf{x}_\ell\|^2-\tau^2\|\mathbf{f}_\ell\|^2}\mathbf{f}_\ell\mathbf{f}_\ell^T & \frac{2\tau\|\mathbf{x}_\ell\|}{\|\mathbf{x}_\ell\|^2-\tau^2\|\mathbf{f}_\ell\|^2}\mathbf{f}_\ell\\ \frac{2\tau\|\mathbf{x}_\ell\|}{\|\mathbf{x}_\ell\|^2-\tau^2\|\mathbf{f}_\ell\|^2}\mathbf{f}_\ell^T & \frac{\|\mathbf{x}_\ell\|^2+\tau^2\|\mathbf{f}_\ell\|^2}{\|\mathbf{x}_\ell\|^2-\tau^2\|\mathbf{f}_\ell\|^2}\end{bmatrix}. \tag{16}$$

Inserting the above $\mathrm{Cay}[\tau\mathbf{A}(\ell)]$ for $\mathbf{G}(\ell)$ into Eq. (13) and taking its first row, we obtain

$$\mathbf{x}_{\ell+1}=\mathbf{x}_\ell+\eta_\ell\mathbf{f}_\ell=\mathbf{x}_\ell+\frac{\|\mathbf{x}_\ell\|^2+\tau\mathbf{f}_\ell\cdot\mathbf{x}_\ell}{\|\mathbf{x}_\ell\|^2-\tau^2\|\mathbf{f}_\ell\|^2}h\mathbf{f}_\ell. \tag{17}$$

In the above $\mathbf{x}_\ell$ denotes the numerical value of $\mathbf{x}$ at the discrete time t_ℓ, τ is one half of the time increment, i.e., $\tau:=h/2$, $\mathbf{f}_\ell$ denotes $\mathbf{f}(\mathbf{x}_\ell,t_\ell)$ for saving notation, and η_ℓ is an adaptive factor.

In order to meet the property (11), we require the time stepsize used in the scheme (17) being constrained by $h<2\|\mathbf{x}_\ell\|/\|\mathbf{f}_\ell\|$. Under this condition we have

$$h<\frac{2\|\mathbf{x}_\ell\|}{\|\mathbf{f}_\ell\|}\Longleftrightarrow G_0^0>0\Longrightarrow\eta_\ell>0. \tag{18}$$

Some properties of preserving the fixed point behavior of the above numerical scheme (17) have been investigated, and applying it to some non-backward problems has revealed that it is easy to implement numerically and has a high computational efficiency and accuracy as discussed by Liu (2001).

2.2 Exponential mapping

An exponential mapping of $\mathbf{A}(\ell)$ admits a closed-form representation:

$$\exp[h\mathbf{A}(\ell)]=\begin{bmatrix}\mathbf{I}_n+\frac{(a_\ell-1)}{\|\mathbf{f}_\ell\|^2}\mathbf{f}_\ell\mathbf{f}_\ell^T & \frac{b_\ell\mathbf{f}_\ell}{\|\mathbf{f}_\ell\|}\\ \frac{b_\ell\mathbf{f}_\ell^T}{\|\mathbf{f}_\ell\|} & a_\ell\end{bmatrix}, \tag{19}$$

where

$$a_\ell:=\cosh\left(\frac{h\|\mathbf{f}_\ell\|}{\|\mathbf{x}_\ell\|}\right),\quad b_\ell:=\sinh\left(\frac{h\|\mathbf{f}_\ell\|}{\|\mathbf{x}_\ell\|}\right). \tag{20}$$

Substituting the above $\exp[h\mathbf{A}(\ell)]$ for $\mathbf{G}(\ell)$ into Eq. (13) and taking its first row, we obtain

$$\mathbf{x}_{\ell+1}=\mathbf{x}_\ell+\eta_\ell\mathbf{f}_\ell, \tag{21}$$

where

$$\eta_\ell := \frac{(a_\ell - 1)\mathbf{f}_\ell \cdot \mathbf{x}_\ell + b_\ell \|\mathbf{x}_\ell\| \|\mathbf{f}_\ell\|}{\|\mathbf{f}_\ell\|^2} \tag{22}$$

is the adaptive factor. From $\mathbf{f}_\ell \cdot \mathbf{x}_\ell \geq -\|\mathbf{f}_\ell\| \|\mathbf{x}_\ell\|$ we can prove that

$$\eta_\ell \geq \frac{\|\mathbf{x}_\ell\|}{\|\mathbf{f}_\ell\|} \left[1 - \exp\left(-\frac{h\|\mathbf{f}_\ell\|}{\|\mathbf{x}_\ell\|} \right) \right] > 0, \ \ \forall h > 0. \tag{23}$$

This scheme is group properties preserved for all $h > 0$, and does not endure the same shortcoming as that for scheme (17).

3 Backward problems and BGPS

3.1 Dynamics on past cone

Corresponding to the initial value problems (IVPs) governed by Eq. (1) with a specified initial value $\mathbf{x}(0)$ at zero time, for many systems in engineering applications, the final value problems (FVPs) may happen due to one wants to retrieve the past histories of states exhibited in the physical models. These time backward problems can be described as

$$\dot{\mathbf{x}} = \mathbf{f}(\mathbf{x}, t), \ \ \mathbf{x} \in \mathbb{R}^n, \ \ t \in \mathbb{R}^-. \tag{24}$$

With a specified final value $\mathbf{x}(0)$ at $t = 0$, we intend to recover the past values of $\mathbf{x}$ in the past time of $t < 0$.

We can embed Eq. (24) into the following $n+1$-dimensional augemented dynamical system:

$$\frac{d}{dt} \begin{bmatrix} \mathbf{x} \\ -\|\mathbf{x}\| \end{bmatrix} = \begin{bmatrix} \mathbf{0}_{n\times n} & -\frac{\mathbf{f}(\mathbf{x},t)}{\|\mathbf{x}\|} \\ -\frac{\mathbf{f}^T(\mathbf{x},t)}{\|\mathbf{x}\|} & 0 \end{bmatrix} \begin{bmatrix} \mathbf{x} \\ -\|\mathbf{x}\| \end{bmatrix}. \tag{25}$$

It is obvious that the first equation in Eq. (25) is the same as the original equation (24), but the inclusion of the second equation gives us a Minkowskian structure of the augmented state variables of $\mathbf{X} := (\mathbf{x}^T, -\|\mathbf{x}\|)^T$ satisfying the cone condition:

$$\mathbf{X}^T \mathbf{g} \mathbf{X} = \mathbf{x} \cdot \mathbf{x} - \|\mathbf{x}\|^2 = \|\mathbf{x}\|^2 - \|\mathbf{x}\|^2 = 0. \tag{26}$$

Here, we should stress that the cone condition imposed on the dynamical system (2) is a future cone as shown in Fig. 1, and that for the dynamical system (25) the imposed cone condition (26) is a past cone as shown in Fig. 1. The so-called future and past are due to the fact that in Eq. (2) the last component of the augmented state vector $\mathbf{X}$ is $\|\mathbf{x}\| > 0$, while that in Eq. (25) the last component of the augmented state vector $\mathbf{X}$ is $-\|\mathbf{x}\| < 0$.

Consequently, we have an $n+1$-dimensional augmented system:

$$\dot{\mathbf{X}} = \mathbf{B}\mathbf{X} \tag{27}$$

with a constraint (26), where

$$\mathbf{B} := \begin{bmatrix} \mathbf{0}_{n\times n} & -\frac{\mathbf{f}(\mathbf{x},t)}{\|\mathbf{x}\|} \\ -\frac{\mathbf{f}^T(\mathbf{x},t)}{\|\mathbf{x}\|} & 0 \end{bmatrix} \tag{28}$$

satisfying

$$\mathbf{B}^T \mathbf{g} + \mathbf{g}\mathbf{B} = \mathbf{0}, \tag{29}$$

is a Lie algebra $so(n,1)$ of the proper orthochronous Lorentz group $SO_o(n,1)$. The term orthochronous used in the special relativity theory is referred to the preservation of time orientation. However, it should be understood here as the preservation of the sign of $-\|\mathbf{x}\|$.

According to the above Lie algebra property of $\mathbf{B}$ we can derive a backward group-preserving scheme as Eq. (13) for Eq. (6):

$$\mathbf{X}_{\ell-1} = \mathbf{G}(\ell)\mathbf{X}_\ell. \tag{30}$$

However, the above one is a backward single-step numerical scheme, which is different from the forward one in Eq. (13). Below we derive two group-preserving schemes for Eq. (27).

3.2 The Cayley transform

The Cayley transform generated from $\mathbf{B} \in so(n,1)$ is

$$\mathrm{Cay}(\tau\mathbf{B}) = (\mathbf{I}_{n+1} - \tau\mathbf{B})^{-1}(\mathbf{I}_{n+1} + \tau\mathbf{B}). \tag{31}$$

Substituting Eq. (28) for $\mathbf{B}(\ell)$ into the above equation yields

$$\mathrm{Cay}[\tau\mathbf{B}(\ell)] = \begin{bmatrix} \mathbf{I}_n + \frac{2\tau^2}{\|\mathbf{x}_\ell\|^2 - \tau^2\|\mathbf{f}_\ell\|^2}\mathbf{f}_\ell\mathbf{f}_\ell^T & -\frac{2\tau\|\mathbf{x}_\ell\|}{\|\mathbf{x}_\ell\|^2 - \tau^2\|\mathbf{f}_\ell\|^2}\mathbf{f}_\ell \\ -\frac{2\tau\|\mathbf{x}_\ell\|}{\|\mathbf{x}_\ell\|^2 - \tau^2\|\mathbf{f}_\ell\|^2}\mathbf{f}_\ell^T & \frac{\|\mathbf{x}_\ell\|^2 + \tau^2\|\mathbf{f}_\ell\|^2}{\|\mathbf{x}_\ell\|^2 - \tau^2\|\mathbf{f}_\ell\|^2} \end{bmatrix}. \tag{32}$$

Inserting the above $\mathrm{Cay}[\tau\mathbf{B}(\ell)]$ for $\mathbf{G}(\ell)$ into Eq. (30) and taking its first row, we obtain

$$\mathbf{x}_{\ell-1} = \mathbf{x}_\ell + \eta_\ell \mathbf{f}_\ell = \mathbf{x}_\ell + \frac{-\|\mathbf{x}_\ell\|^2 + \tau\mathbf{f}_\ell \cdot \mathbf{x}_\ell}{\|\mathbf{x}_\ell\|^2 - \tau^2\|\mathbf{f}_\ell\|^2} h\mathbf{f}_\ell. \tag{33}$$

In order to meet the property (11), the time stepsize is constrained by $h < 2\|\mathbf{x}_\ell\|/\|\mathbf{f}_\ell\|$. Under this condition we have

$$h < \frac{2\|\mathbf{x}_\ell\|}{\|\mathbf{f}_\ell\|} \Longleftrightarrow G_0^0 > 0 \Longrightarrow \eta_\ell < 0. \tag{34}$$

3.3 Exponential mapping

An exponential mapping of $\mathbf{B}(\ell)$ admits a closed-form representation:

$$\exp[h\mathbf{B}(\ell)] = \begin{bmatrix} \mathbf{I}_n + \frac{(a_\ell-1)}{\|\mathbf{f}_\ell\|^2}\mathbf{f}_\ell\mathbf{f}_\ell^T & -\frac{b_\ell\mathbf{f}_\ell}{\|\mathbf{f}_\ell\|} \\ -\frac{b_\ell\mathbf{f}_\ell^T}{\|\mathbf{f}_\ell\|} & a_\ell \end{bmatrix}, \tag{35}$$

where a_ℓ and b_ℓ were defined by Eq. (20).

Substituting the above $\exp[h\mathbf{B}(\ell)]$ for $\mathbf{G}(\ell)$ into Eq. (30) and taking its first row, we obtain

$$\mathbf{x}_{\ell-1} = \mathbf{x}_\ell + \eta_\ell\mathbf{f}_\ell, \tag{36}$$

where

$$\eta_\ell := \frac{(a_\ell-1)\mathbf{f}_\ell\cdot\mathbf{x}_\ell - b_\ell\|\mathbf{x}_\ell\|\|\mathbf{f}_\ell\|}{\|\mathbf{f}_\ell\|^2}. \tag{37}$$

From $\mathbf{f}_\ell\cdot\mathbf{x}_\ell \le \|\mathbf{f}_\ell\|\|\mathbf{x}_\ell\|$ it follows that

$$\eta_\ell \le \frac{\|\mathbf{x}_\ell\|}{\|\mathbf{f}_\ell\|}\left[\exp\left(-\frac{h\|\mathbf{f}_\ell\|}{\|\mathbf{x}_\ell\|}\right)-1\right] < 0, \ \ \forall h > 0. \tag{38}$$

This scheme is group properties preserved for all $h > 0$, and does not endure the same shortcoming as that for scheme (33).

Comparing Eqs. (33) and (17) it is interesting to note that these two numerical schemes have the same form in addition that the sign before $\|\mathbf{x}_\ell\|$ in the numerators. Similarly, Eqs. (37) and (22) have the same form in addition that the sign before $b_\ell\|\mathbf{x}_\ell\|\|\mathbf{f}_\ell\|$ in the numerators. In the Appendix we derive the above two numerical schemes by a different approach. In the later we will call these numerical schemes the backward group preserving scheme (BGPS), in order to differentiate them from the group preserving scheme (GPS) introduced in Section 2 for the forward differential dynamics. On the other hand, in the whole calculations of the BHCP in Section 5 we will employ the exponential mapping BGPS, for the above reason of group properties preserved for all $h > 0$ of this numerical method.

4 Numerical examples of backward ODEs

In this section we apply schemes (33) and (36) to backward ODEs, which have closed-form solutions. Our purpose is to test the performance of the newly-developed numerical methods.

4.1 Example 1

Consider the following planar dynamical system:

$$\dot{x}_1 = -x_1 + \frac{2x_2}{\ln(x_1^2+x_2^2)}, \ \ \dot{x}_2 = -x_2 - \frac{2x_1}{\ln(x_1^2+x_2^2)}, \ \ t \ge 0, \tag{39}$$

whose solution, in terms of the polar coordinates (r,θ), can be expressed as

$$r(t) = r_0 e^{-t}, \ \ \theta(t) = \theta_0 + \ln\left(1 - \frac{t}{\ln r_0}\right),$$

where $r_0 = r(0)$ and $\theta_0 = \theta(0)$ are initial values.

This example is not a backward problem; however, we use it to demonstrate the accuracy of schemes (33) and (36) by specifying terminal conditions at $t = T$:

$$x_1(T) = r_0 e^{-T}\cos\left(\theta_0 + \ln\left[1 - \frac{T}{\ln r_0}\right]\right), \tag{40}$$

$$x_2(T) = r_0 e^{-T}\sin\left(\theta_0 + \ln\left[1 - \frac{T}{\ln r_0}\right]\right). \tag{41}$$

Applying schemes (33) and (36) to Eq. (39) in the time interval of $2 \ge t > 0$ sec with a time stepsize of $h = 0.001$ sec, and under the above terminal conditions with $r_0 = 10$ and $\theta_0 = \pi/6$, the numerical results indicate that the accuracy of both schemes is in the order of 10^{-2} for x_1 and 10^{-3} for x_2 as shown in Fig. 2(a) and (b). The errors were obtained by taking the absolute of the differences between exact solutions and numerical solutions. We also plotted η/h in Fig. 2(c), from which it can be seen that the values of η/h for these two schemes are slightly different.

4.2 Example 2

In this example, we consider the Euler equations of rigid body dynamics:

$$\frac{d}{dt}\begin{bmatrix}\Pi_1\\ \Pi_2\\ \Pi_3\end{bmatrix} = \begin{bmatrix} 0 & \frac{\Pi_3}{I_3} & \frac{-\Pi_2}{I_2} \\ \frac{-\Pi_3}{I_3} & 0 & \frac{\Pi_1}{I_1} \\ \frac{\Pi_2}{I_2} & \frac{-\Pi_1}{I_1} & 0 \end{bmatrix}\begin{bmatrix}\Pi_1\\ \Pi_2\\ \Pi_3\end{bmatrix}, \tag{42}$$

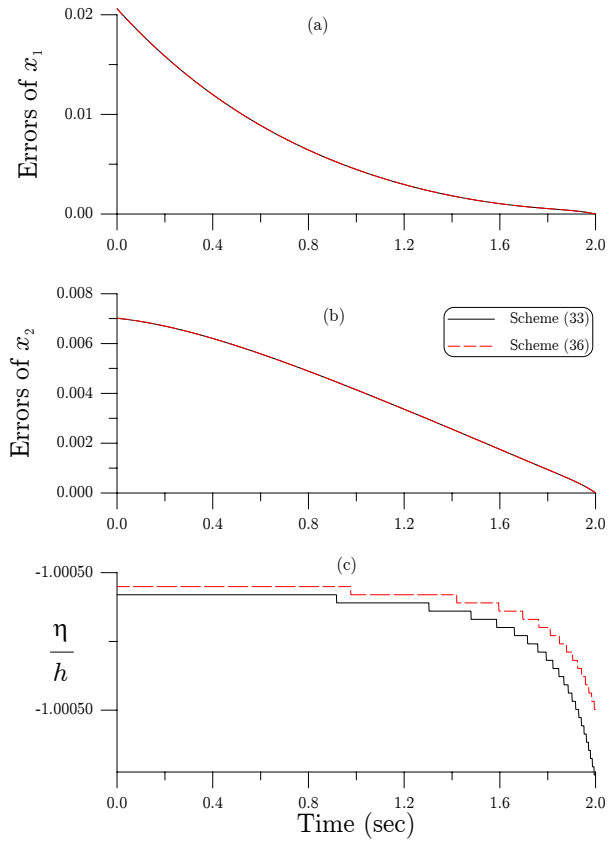

Figure 2 : Applying schemes (33) and (36) to Example 1: (a) the errors of x_1, (b) the errors of x_2, and (c) the time histories of η/h.

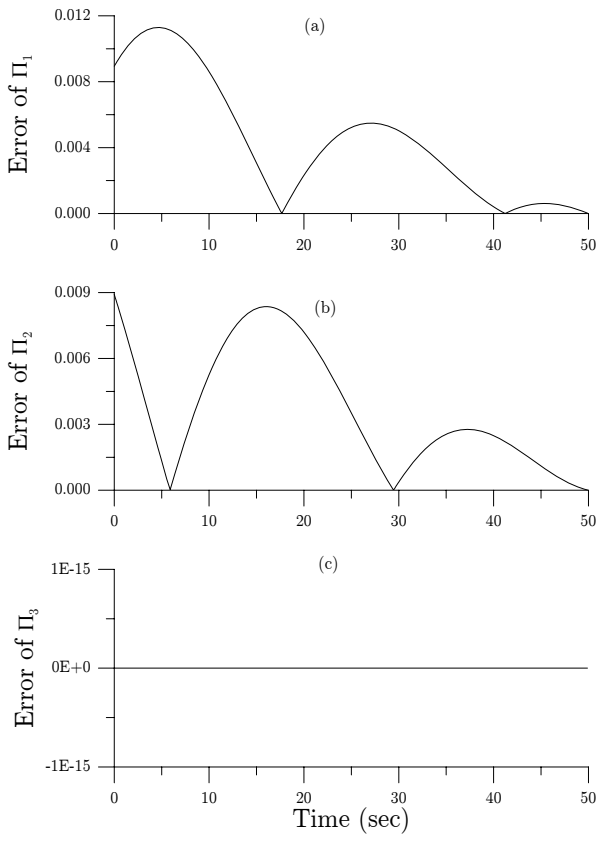

Figure 3 : Applying scheme (36) to Example 2: (a) the error of Π_1, (b) the error of Π_2, and (c) the error of Π_3.

where $I_1, I_2, I_3 > 0$ are the three principal moments of inertia of the body, and Π_1, Π_2, Π_3 are the three components of body angular momentum.

For the special case $I_1 = I_2 > I_3$, the closed-form solution of Euler equations is available [see, e.g., Marsden and Ratiu (1994)]:

$$\begin{aligned}
\Pi_1(t) &= \Pi_1(0)\cos\frac{(I_3-I_1)\Pi_3(0)}{I_1 I_3}t \\
&\quad -\Pi_2(0)\sin\frac{(I_3-I_1)\Pi_3(0)}{I_1 I_3}t, \\
\Pi_2(t) &= \Pi_2(0)\cos\frac{(I_3-I_1)\Pi_3(0)}{I_1 I_3}t \\
&\quad +\Pi_1(0)\sin\frac{(I_3-I_1)\Pi_3(0)}{I_1 I_3}t, \\
\Pi_3(t) &= \Pi_3(0).
\end{aligned} \tag{43}$$

We use this example to demonstrate the accuracy of schemes (33) and (36) by specifying terminal conditions at $T = 50$ sec calculated from above equations. We fix $I_1 = I_2 = 5$ and $I_3 = 3$ and $\Pi_1(0) = \Pi_2(0) = \Pi_3(0) = 1$ in the calculation. Applying scheme (36) to Eq. (42) in the time interval of $50 \geq t \geq 0$ sec with a time stepsize of $h = 0.02$ sec, the numerical results as shown in Fig. 3 indicate that the accuracy of BGPS is in the order of 10^{-2} for Π_1, 10^{-3} for Π_2 and no error for Π_3.

5 Backward heat conduction problems

5.1 *The governing equation*

The BHCP we consider is

$$\frac{\partial u}{\partial t} = \nu \triangle u \ \text{ in } \ \Omega, \tag{44}$$

$$u = u_{\rm B} \ \text{ on } \ \Gamma_{\rm B}, \tag{45}$$

$$u = u_{\rm F} \ \text{ on } \ \Gamma_{\rm F}, \tag{46}$$

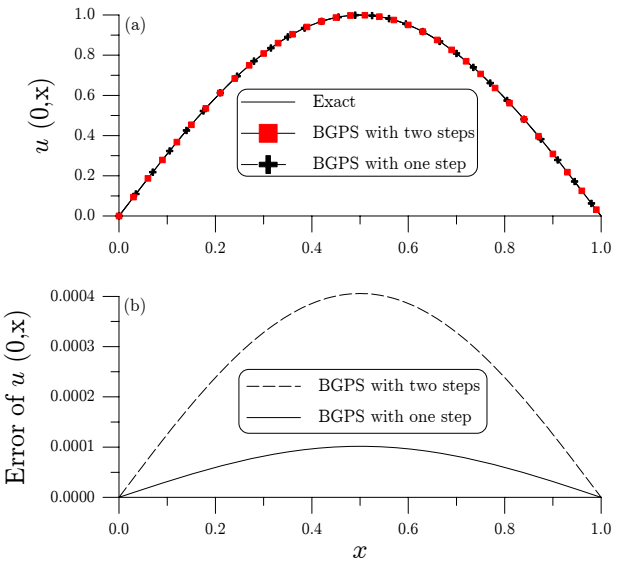

Figure 4 : Applying scheme (36) to Example 3: (a) comparing one-step and two-step BGPS solutions with exact solution, and (b) the numerical errors of $u(0,x)$.

where u is a scalar temperature field of heat distribution and ν is the heat diffusion coefficient. We take a bounded domain D in $\mathbb{R}^k$ and a spacetime domain $\Omega = D \times (0,T)$ in $\mathbb{R}^{k+1}$ for a final time $T > 0$, and write two surfaces $\Gamma_B = \partial D \times [0,T]$ and $\Gamma_F = D \times \{T\}$ of the boundary $\partial\Omega$. $\triangle$ denotes the k-dimensional Laplacian operator. Eqs. (44)-(46) constitute a k-dimensional backward heat conduction problem for a given boundary data $u_B : \Gamma_B \mapsto \mathbb{R}$ and a final data $u_F : \Gamma_F \mapsto \mathbb{R}$.

It is well known that the approach of ill-posed problems by numerical method is rather difficult [Han, Ingham and Yuan (1995); Mera, Elliott, Ingham and Lesnic (2001); Mera, Elliott and Ingham (2002); Kirkup and Wadsworth (2002); Liu (2002); Chiwiacowsky and de Campos Velho (2003); Iijima (2004); Liu (2004); Mera (2005)]. For example, for any time stepsize $h > 0$ and for any lattice spacing lengths $\Delta x_1 > 0, \ldots, \Delta x_k > 0$, it is known that the finite-difference scheme for Eq. (44) is unstable even under the von Neumann condition, which is a necessary numerical stability condition for the forward finite difference scheme of initial-value problem.

Here we are going to calculate the BHCP by a semi-discretization method, which replaces Eq. (44) by a set of ODEs:

$$\frac{\partial u(x_1,\ldots,x_k,t)}{\nu \partial t} = \{u(x_1+\Delta x_1,\ldots,x_k,t) - 2u(x_1,\ldots,x_k,t) + u(x_1-\Delta x_1,\ldots,x_k,t)\}/(\Delta x_1)^2 + \cdots + \{u(x_1,\ldots,x_k+\Delta x_k,t) - 2u(x_1,\ldots,x_k,t) + u(x_1,\ldots,x_k-\Delta x_k,t)\}/(\Delta x_k)^2 \quad (47)$$

at the interior grid points in the domain D, together with the backward group preserving schemes (BGPS) developed in Section 3 for the resulting backward ODEs.

5.2 *Example 3*

In order to compare our numerical results with those obtained by Lesnic, Elliott and Ingham (1998), Mera, Elliott, Ingham and Lesnic (2001), Mera, Elliott and Ingham (2002) and Mera (2005), let us first consider a one-dimensional benchmark BHCP:

$$u_t = u_{xx}, \quad 0 < x < 1, \quad 0 < t < T, \quad (48)$$

with the boundary conditions

$$u(0,t) = u(1,t) = 0, \quad (49)$$

and the final time condition

$$u(x,T) = \sin(\pi x)\exp(-\pi^2 T). \quad (50)$$

The data to be retrieved is given by

$$u(x,t) = \sin(\pi x)\exp(-\pi^2 t), \quad T > t \geq 0. \quad (51)$$

The one-dimensional spatial domain $[0,1]$ is discretized by $N = n+2$ points including two end points, at which the two boundary conditions $u_0(t) = u_{n+1}(t) = 0$ are imposed on the totally n differential equations obtained from Eq. (47) by considering $k = 1$. We apply the BGPS developed in Section 3.3 for this backward problem of n differential equations with the final data given by Eq. (50).

When $T = 0.5$ sec, we compare two computations in Fig. 4: one with $n = 99$, i.e. $\Delta x = 1/100$, and $h = 0.25$ sec, and another one with $n = 199$, i.e. $\Delta x = 1/200$, and $h = 0.5$ sec. The first computation with two steps and the latter one with only a one-step. From Fig. 4(a) it can be seen that the computed data at the grid points are almost located on the sine curve obtained from Eq. (51)

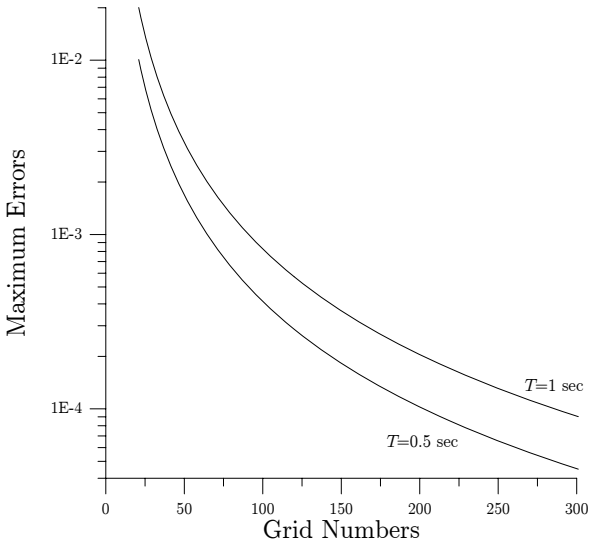

Figure 5 : The maximum error as a function of the number of grid points for the final times of $T = 1$ sec and $T = 0.5$ sec.

with $t = 0$. It is hardly to see the difference of these two numerical solutions with the exact solution. Therefore, we plot the numerical error defined by taking the absolute of the difference of numerical results with exact data in Fig. 4(b). After viewing the output data we were seen that the error is rather smaller with a maximum 0.000405776 for the two-step BGPS, and encouragingly small for the one-step BGPS with a maximum 0.000101462, where the maximum error is defined as

$$\text{Maximum Error} := \text{Max}_{i\in\{1,\ldots,N\}}|u_i - \sin \pi x_i|,$$

where N is the total grid point, and u_i denotes the numerical value of u at the i-th grid point with a position $x = x_i$. Even under the same $\Delta x = 1/100$, the one-step BGPS is accurate as that uses two-step.

The computational results strongly support us to use a one-step BGPS with a finer grid length to compute the BHCP of this example. On the other hand, there are five reasons for a one-step BGPS: (a) as mentioned in Section 3.3 the BGPS is group properties preserved for all $h > 0$; (b) when the number of grid points increases the BGPS with multiple steps may cause instability of the numerical solution; (c) a one-step computation is much time saving; (d) there has no error propagation of the one-step computation; (e) it can increase the spatial resolution by increasing the number of grid points.

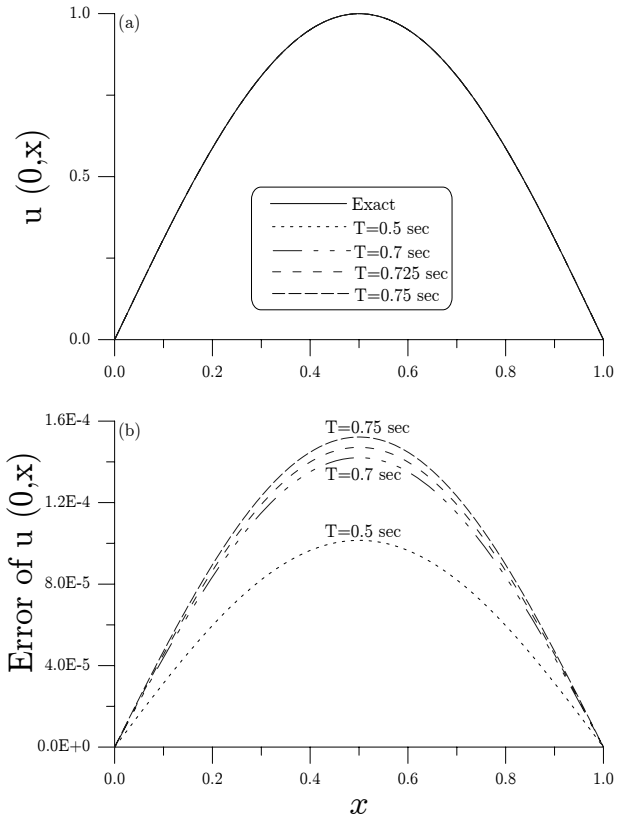

Figure 6 : The comparison of exact solutions and numerical solutions for Example 3 were made in (a) with different final times of $T = 0.5, 0.7, 0.725, 0.75$ sec, and (b) the errors of numerical solutions.

Next we investigate the influence of the number of grid points on the accuracy for two cases $T = 0.5$ sec and $T = 1$ sec in Fig. 5. It can be seen that more grid points can increase the accuracy. However, it was found that even for small numbers of grid point the one-step BGPS can produce a rather accurate numerical solution.

In Fig. 6 we show the numerical results and numerical errors for different final times of $T = 0.5, 0.7, 0.725, 0.75$ sec. They are also calculated by BGPS with one step but keeping $\Delta x = 1/200$. Upon compared with the numerical results computed by Mera (2005) with the method of fundamental solution (MFS) together with Tikhonov regularization technique (see Figure 5 of the above cited paper), we can say that BGPS is much accurate than MFS.

Let us further investigate some very severely ill-posed cases of this benchmark BHCP, where $T = 1.5, 2, 2.2, 2.4$ sec were employed, such that when the fi-

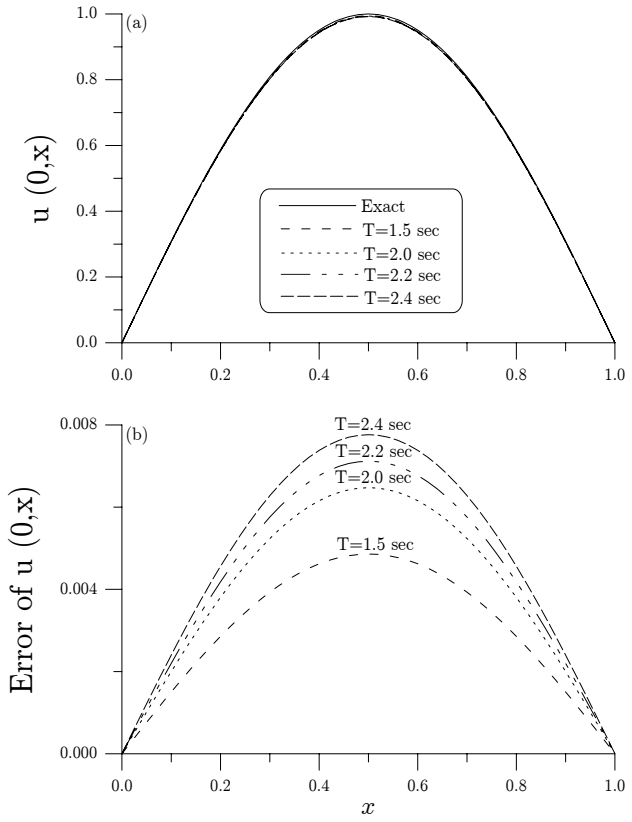

Figure 7 : The comparison of exact solutions and numerical solutions for Example 3 were made in (a) with different final times of $T = 1.5, 2, 2.2, 2.4$ sec, and (b) the errors of numerical solutions.

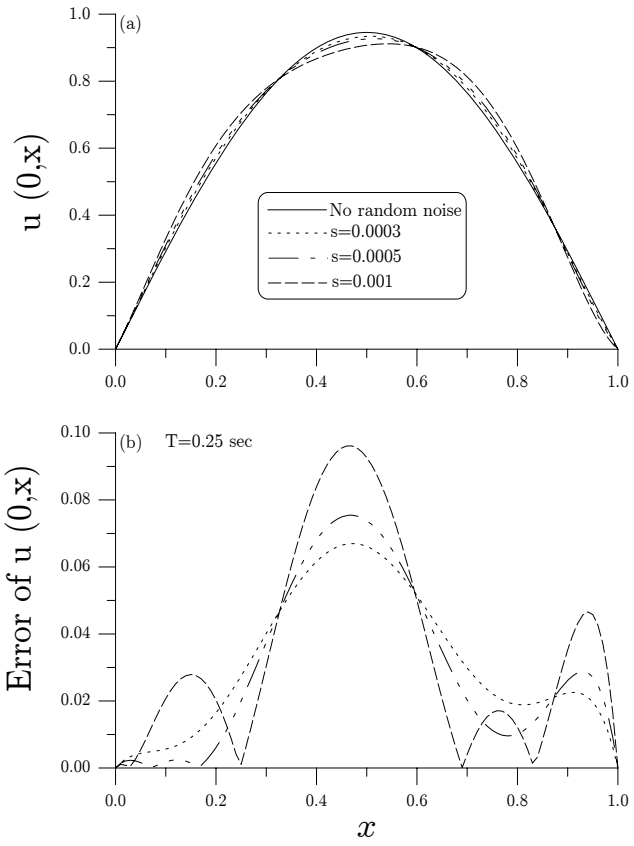

Figure 8 : The comparison of numerical solutions for Example 3 were made in (a) with different levels of noise $s = 0, 0.001, 0.0003, 0.0005$, and (b) the corresponding numerical errors.

nal data are in the order of $O(10^{-7}) - O(10^{-11})$ we want to use BGPS to retrieve the desired initial data $\sin \alpha x$, which is in the order of $O(1)$. For this very difficult problem, the method proposed by Lesnic, Elliott and Ingham (1998) was instable when $T > 1$ sec. However, the results given by BGPS with $\Delta x = 1/200$ and one step, i.e. $h = T$, in the calculations are free of such difficulty and we were able to retrieve the desired initial data rather accurately as shown in Fig. 7. Even for the severe case up to $T = 2.4$ sec, our computation is stable, and the maximum error occurring at $x = 0.5$ is about 0.008.

To the authors' best knowledge, there has no report that the numerical methods for this severely ill-posed BHCP can provide more accurate results than us.

In the case when the input final measured data are contaminated by random noise, we are concerned with the stability of BGPS, which is investigated by adding the different levels of random noise on the final data. We use the function RANDOM_NUMBER given in Fortran to generate the noisy data $R(i)$, where $R(i)$ are random numbers in $[-1, 1]$. The numerical results with $T = 0.25$ sec were compared with the numerical result without considering random noise in Fig. 8. The noise is obtained by multiplying $R(i)$ by a factor s. It can be seen that the noise levels with $s = 0.0003, 0.0005, 0.001$ disturb the numerical solutions deviating from the exact solution small.

5.3 Example 4

Let us consider the one-dimensional BHCP:

$$u_t = \nu u_{xx}, \quad 0 < x < 1, \quad 0 < t < T, \tag{52}$$

with the boundary conditions

$$u(0,t) = u(1,t) = 0, \tag{53}$$

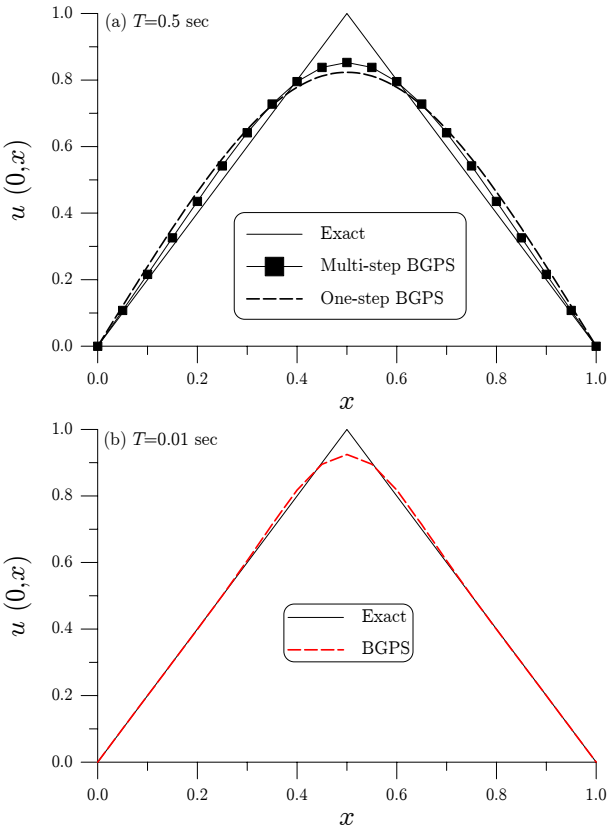

Figure 9 : For Example 4 we compare one-step and multi-step BGPS solutions with exact solution with $T = 0.5$ sec in (a), and multi-step BGPS solution with exact solution with $T = 0.01$ sec in (b).

and the initial condition

$$u(x,0) = \begin{cases} 2x, & \text{for } 0 \le x \le 0.5, \\ 2(1-x), & \text{for } 0.5 \le x \le 1. \end{cases} \tag{54}$$

The exact solution is given by

$$u(x,t) = \sum_{k=0}^{\infty} \frac{8}{\pi^2(2k+1)^2} \cos\frac{(2k+1)\pi(2x-1)}{2} \times \exp[-\pi^2 \nu (2k+1)^2 t]. \tag{55}$$

The backward numerical solution is subjected to the final condition at time T:

$$u(x,T) = \sum_{k=0}^{\infty} \frac{8}{\pi^2(2k+1)^2} \cos\frac{(2k+1)\pi(2x-1)}{2} \times \exp[-\pi^2 \nu (2k+1)^2 T]. \tag{56}$$

In practice, the data is obtained by taking the sum of the first two hundred terms, which guarantees the convergence of the series.

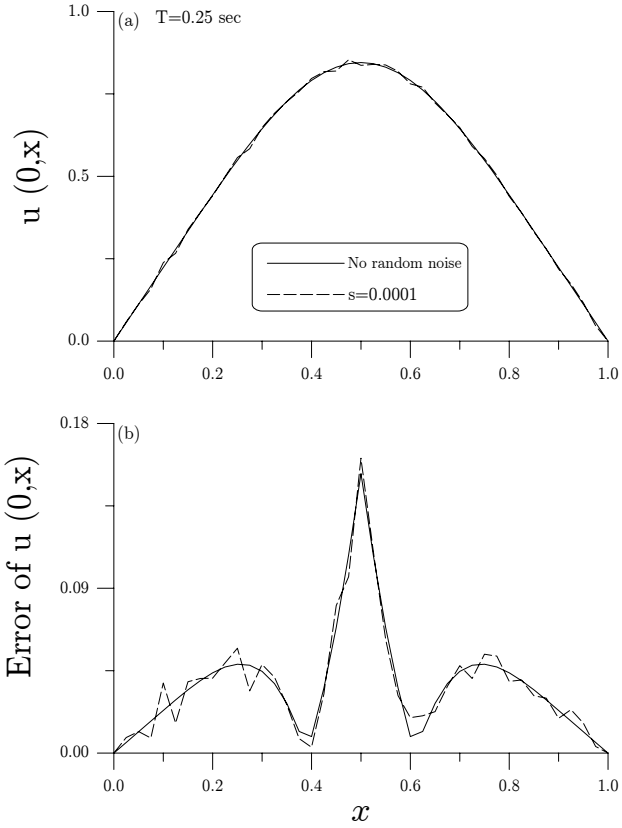

Figure 10 : The comparison of BGPS solutions with and without random noise effect for Example 4 were plotted in (a), and the corresponding errors of $u(0,x)$ were plotted in (b).

The difficulty of this problem is originated from that we use a smooth final data to retrieve a non-smooth initial data. In the literature, this one-dimensional BHCP is called a triangular test [Muniz, de Campos Velho and Ramos (1999); Muniz, Ramos and de Campos Velho (2000); Chiwiacowsky and de Campos Velho (2003)].

For this computational example we have taken $\nu = 0.1$, $n = 19$, $T = 0.5$ sec, $h = 0.05$ sec and $\Delta x = 1/20$. The accuracy as can be seen from Fig. 9(a) is rather good besides that at the turning point $x = 0.5$. We also calculate this example by the one-step BGPS, i.e. $h = 0.5$ sec, and with $\Delta x = 1/40$. It is very interesting that the one-step solution is very near to the multi-step solution.

Muniz, de Campos Velho and Ramos (1999) and Muniz, Ramos and de Campos Velho (2000) have calcu-

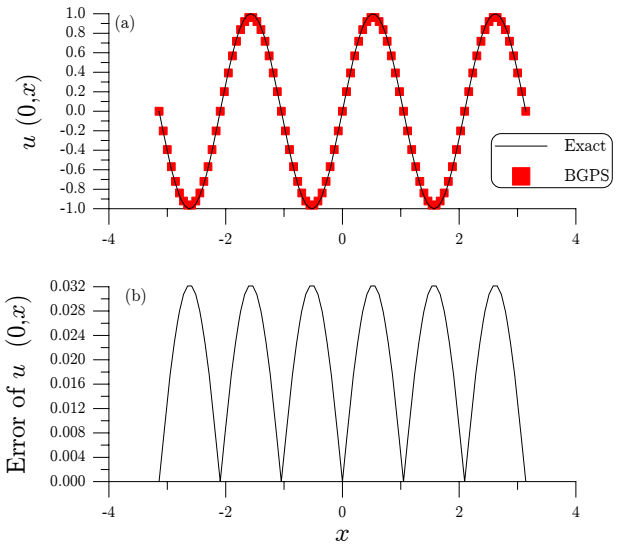

Figure 11 : For Example 5 we compare BGPS solution with exact solution with $T = 1$ sec in (a), and the numerical error of $u(0,x)$ in (b).

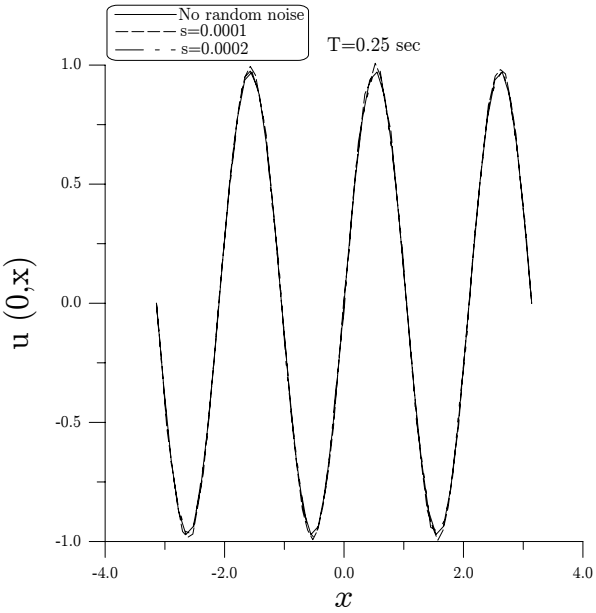

Figure 12 : For Example 5 we compare the BGPS solutions with different levels of noise $s = 0, 0.0001, 0.0002$ for $T = 0.25$ sec.

lated this example by different regularization techniques. They have shown that the explicit inversion method does not give satisfactory results even with a small terminal time with $T = 0.008$ sec [Muniz, de Campos Velho and Ramos (1999)]. Muniz, Ramos and de Campos Velho (2000) have calculated the initial data with a terminal time $T = 0.01$ sec by Tikhonov regularization, maximum entropy principle and truncated singular value decomposition, and good results were obtained as shown in Figures 4 and 5 of the above cited paper. However, when we apply BGPS to this problem with $\nu = 1$, $T = 0.01$ sec, $h = 0.0005$ sec and $\Delta x = 1/40$, more accurate result can be seen from Fig. 9(b). The maximum error occurring at $x = 0.5$ is 0.0619522.

For this example with $T = 0.25$ sec, the comparison of BGPS solutions with and without considering random noise effect were also plotted in Fig. 10(a), and the corresponding errors of $u(0,x)$ were plotted in Fig. 10(b).

5.4 Example 5

Let us consider the third example of one-dimensional BHCP:

$$u_t = u_{xx}, \quad -\pi < x < \pi, \quad T > t > 0, \tag{57}$$

with the boundary conditions

$$u(-\pi,t) = u(\pi,t) = 0, \tag{58}$$

and the final time condition

$$u(x,T) = e^{-\alpha^2 T}\sin\alpha x. \tag{59}$$

The exact solution is given by

$$u(x,t) = e^{-\alpha^2 t}\sin\alpha x, \tag{60}$$

where $\alpha \in \mathbb{N}$ is a positive integer.

We can demonstrate this ill-posed problem further by considering the L^2-norms of u and its final data:

$$\begin{aligned}\|u(x,t)\|_{L^2}^2 &= \int_0^T \int_{-\pi}^{\pi} (e^{-\alpha^2 t}\sin\alpha x)^2 dxdt \\ &= \frac{1}{2\alpha^2}(e^{2\alpha^2 T} - 1)\int_{-\pi}^{\pi}(e^{-\alpha^2 T}\sin\alpha x)^2 dx. \end{aligned} \tag{61}$$

Since for any $C > 0$ there exists $\alpha \in \mathbb{N}$ such that $\sqrt{e^{2\alpha^2 T} - 1}/(\sqrt{2}\alpha) > C$, an inequality $\|u(x,t)\|_{L^2} > C\|u_{\mathrm{F}}\|_{L^2}$ holds for any $C > 0$. This means that the solution does not depend on the final data continuously. Therefore, the BHCP is unstable for a given final data with respect to the L^2-norm. Larger α is, more worse is

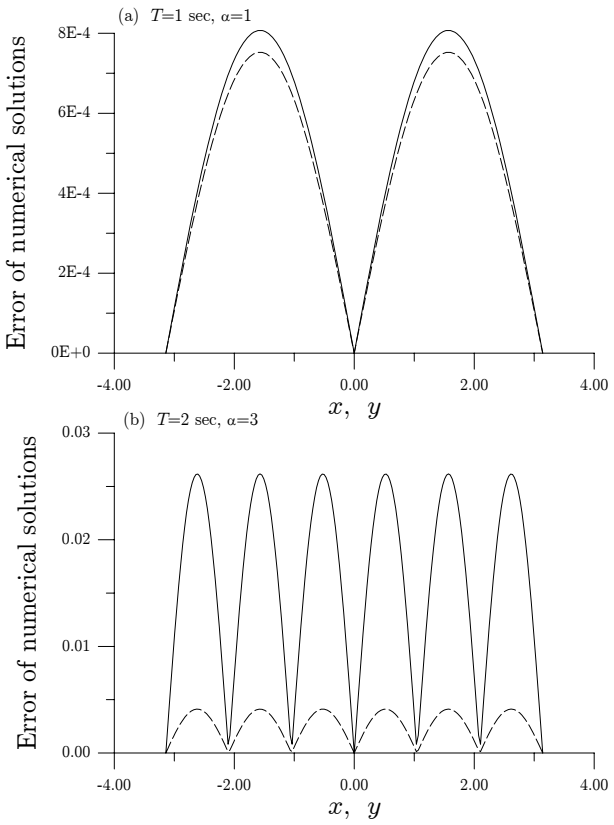

Figure 13 : The errors of BGPS solutions for Example 6 are plotted in (a) with $T = 1$ sec and $\alpha = 1$, and in (b) with $T = 2$ sec and $\alpha = 3$.

the final data dependence on the solution. In other words, the problem is more ill-posed when α is larger.

In Fig. 11 we show the numerical results which being compared with the exact solution (60) at time $t = 0$ for the case of $\alpha = 3$ and $T = 1$ sec. In the calculation, the grid length was taken to be $\Delta x = 2\pi/90$ and the time step-size was taken to be $h = 1$ sec.

Due to the rather small final data in the order of $O(10^{-4})$ when comparing with the desired initial data $\sin\alpha x$ of order $O(1)$ to be retrieved, Mera (2005) has mentioned that it is impossible to solve this strongly ill-posed problem by using classical numerical methods and requires special techniques to be employed. However, by using the one-step BGPS method we can treat this problem very good as shown in Fig. 11(a), and the numerical error is very small in the order $O(10^{-2})$ as shown in Fig. 11(b). In Fig. 12 we calculate this example with $T = 0.25$ sec under the noise level of $s = 0.0001$ by using the grid length $\Delta x = 2\pi/72$ and under $s = 0.0002$ by using the grid length $\Delta x = 2\pi/52$. It can be seen that the numerical method of one-step BGPS is robust to against the noise disturbance.

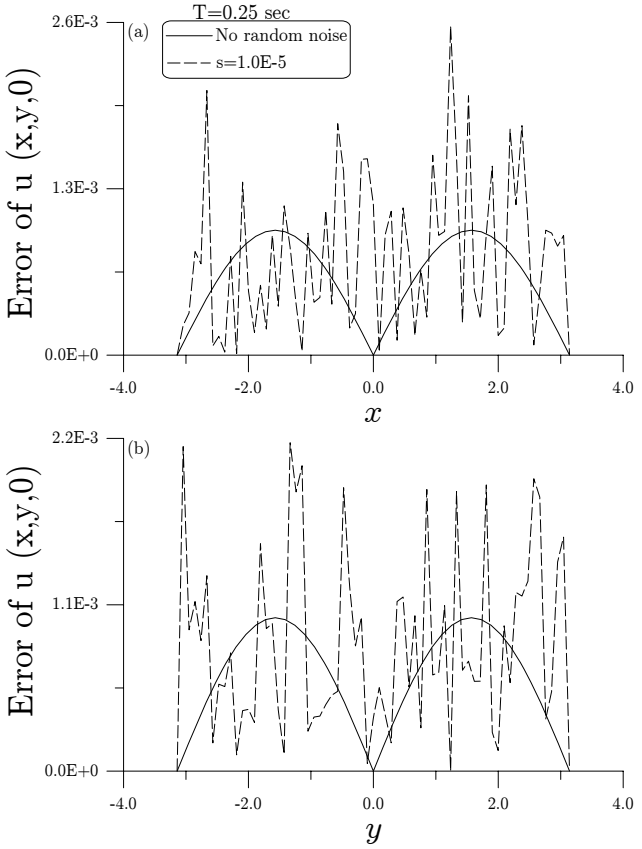

Figure 14 : The numerical errors of BGPS solutions with and without random noise effect for Example 6 were plotted in (a) with respect to x at fixed $y = 2\pi/3$, and in (b) with respect to y at fixed $x = \pi/2$.

5.5 Example 6

Let us consider the first example of two-dimensional BHCP:

$$u_t = u_{xx} + u_{yy}, \quad -\pi < x < \pi, \quad -\pi < y < \pi, \quad T > t > 0, \tag{62}$$

with the boundary conditions

$$u(-\pi, y, t) = u(\pi, y, t) = u(x, -\pi, t) = u(x, \pi, t) = 0, \tag{63}$$

and the final time condition

$$u(x, y, T) = e^{-2\alpha^2 T} \sin\alpha x \sin\alpha y. \tag{64}$$

The exact solution is given by

$$u(x,y,t) = e^{-2\alpha^2 t}\sin\alpha x \sin\alpha y, \tag{65}$$

where $\alpha \in \mathbb{N}$ is a positive integer.

In Fig. 13(a) we show the errors of numerical solutions obtained from the BGPS for the case of $\alpha = 1$. $T = 1$ sec was used in this comparison, where the grid lengths were taken to be $\Delta x = \Delta y = 2\pi/90$, and the time stepsize was taken to be $h = 1$ sec. At the point $x = -\pi + 134\pi/90$ the error is plotted with respect to y by a dashed line, and at the point $y = -\pi + 148\pi/90$ the error is plotted with respect to x by a solid line. The latter one is smaller than the former one because the point $y = -\pi + 148\pi/90$ is near to the boundary. The errors however are much smaller than that calculated by Liu (2004) as shown in Figure 4 therein.

Clearly, if T in Eq. (64) is chosen sufficiently large, such that the order of $u(x,y,T)$ decreases below our computer machine precision then the BCHP of this example will become uncomputable. In order to give a stringent test of the BGPS when applied it on this example, we let $\alpha = 3$ and $T = 2$ sec. The final data is very small in the order of $O(10^{-16})$, which is almost uncomputable by our PC. However, we can use the BGPS to retrieve the desired initial data $\sin\alpha x \sin\alpha y$, which is in the order of $O(1)$. The errors of numerical solutions calculated by BGPS with $\Delta x = \Delta y = 2\pi/200$ and one step in the calculation were shown in Fig. 13(b), where at the point $x = -\pi + 300\pi/200$ the error is plotted with respect to y by a dashed line, and at the point $y = -\pi + 332\pi/200$ the error is plotted with respect to x by a solid line. For this very difficult problem, the BGPS method proposed here is also good with a maximum error 0.026288.

In Fig. 14 we compare the numerical errors with $T = 0.25$ sec for two cases: one without random noise and another one with random noise in the level of $s = 10^{-5}$. The exact solution and numerical solutions were plotted in Fig. 15(a)-(c) sequentially. Even under the noise the numerical solution displayed in Fig. 15(c) is a good approximation to the exact initial data as shown in Fig. 15(a).

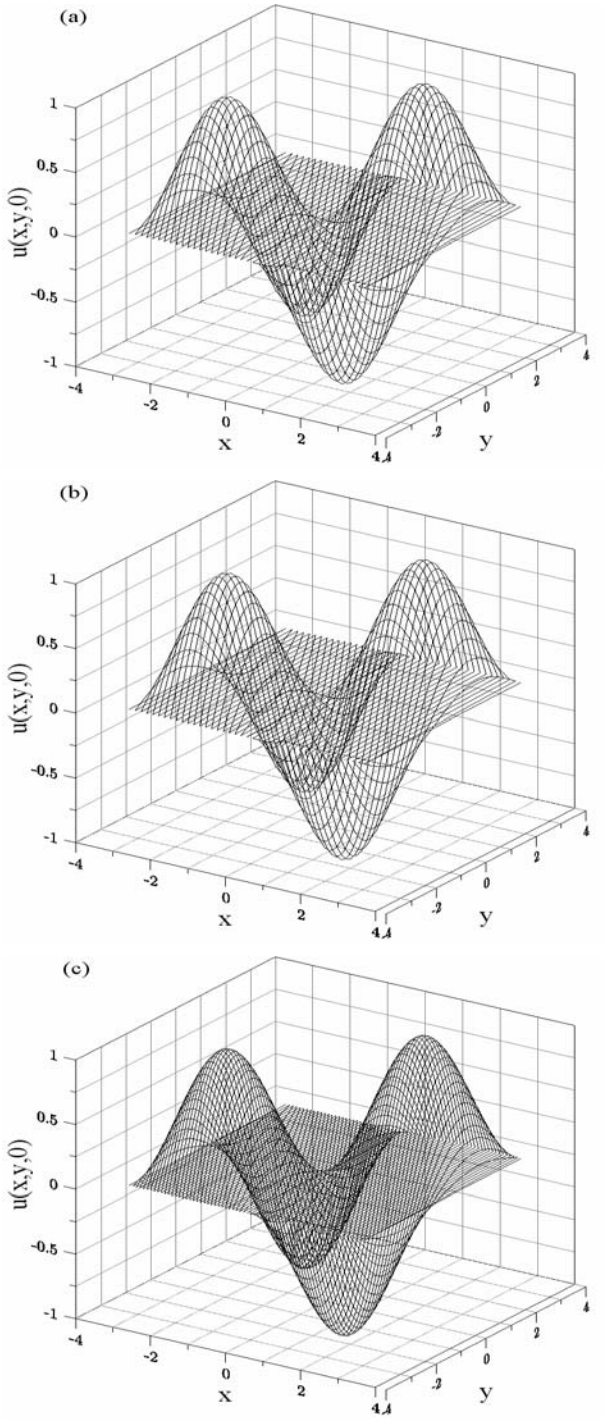

Figure 15 : The exact solution for Example 6 of two-dimensional BHCP were plotted in (a), in (b) the BGPS solution without random noise effect, and in (c) the BGPS solution with random noise.

5.6 Example 7

Let us consider the second example of two-dimensional BHCP [Mera (2005)]:

$$u_t = \frac{1}{2}[u_{xx} + u_{yy}], \ 0 < x < 1, \ 0 < y < 1, \ T > t > 0, \tag{66}$$

with the time varying boundary conditions

$$u(0,y,t) = e^{-\pi^2 t}\sin\pi(y-1), \ \ u(1,y,t) = e^{-\pi^2 t}\sin\pi y, \tag{67}$$

$$u(x,0,t) = e^{-\pi^2 t}\sin\pi(x-1), \ \ u(x,1,t) = e^{-\pi^2 t}\sin\pi x, \tag{68}$$

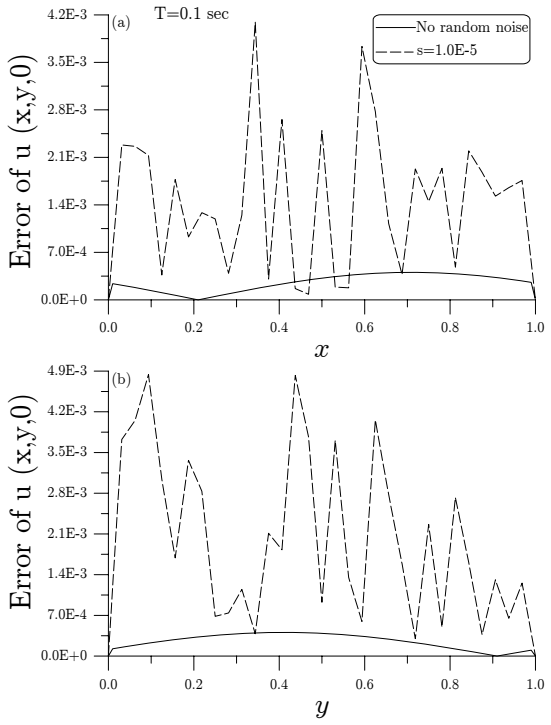

Figure 16 : The errors of BGPS solutions with and without random noise effect for Example 7 were plotted in (a) with respect to x at fixed $y = 0.8$, and in (b) with respect to y at fixed $x = 0.1$.

and the final time condition

$$u(x,y,T) = e^{-\pi^2 T} \sin\pi(x+y-1). \tag{69}$$

The exact solution is given by

$$u(x,y,t) = e^{-\pi^2 t} \sin\pi(x+y-1). \tag{70}$$

In Fig. 16 we compare the numerical errors with $T = 0.1$ sec for two cases: one without random noise and another one with random noise in the level of $s = 10^{-5}$, where the grid lengths were taken to be $\Delta x = \Delta y = 1/50$, and the time stepsize was taken to be $h = 0.1$ sec. At the point $y = 0.8$ the errors were plotted with respect to x in Fig. 16(a), and at the point $x = 0.1$ the errors were plotted with respect to y in Fig. 16(b).

6 Conclusions

The heat conduction problems are calculated by the formulation with a semi-discretization of heat conducting equations in conjuction with the group preserving numerical integration scheme. As well known, in the backward numerical integration of the heat conduction equations a simple employment of the finite difference or finite element method with negative time steps is numerically unstable. In this paper we were concerned with this numerical integration problem, in which the key point was the construction of a past cone and a backward group preserving scheme. It is a first time that we could construct a geometry (past cone), algebra (Lie algebra) and group (Lie group) description of the backward problems governed by differential equations.

By employing the BGPS we can recover all initial data with high order accuracy. Several numerical examples of the BHCP were work out, which show that our numerical integration methods are applicable to the BHCP, even for the very strongly ill-posed ones. Under the noised final data the BGPS was also robust enough to retrieve the initial data. In the most computations of the BHCP, a one-step BGPS was applicable to recover the initial data, having a higher accuracy with a suitable finer grid length. This is especially true when the initial data to be retrieved are smooth. The efficiency of one-step BGPS was rooted in the closure property of the Lie group that we used it to construct the numerical method for BHCP.

References

Chang, C.-W.; Liu, C.-S.; Chang, J.-R. (2005): A group preserving scheme for inverse heat conduction problems. *CMES: Computer Modeling in Engineering & Sciences*, in press.

Chiwiacowsky, L. D.; de Campos Velho, H. F. (2003): Different approaches for the solution of a backward heat conduction problem. *Inv. Prob. Eng.*, vol. 11, pp. 471-494.

Han, H.; Ingham, D. B.; Yuan, Y. (1995): The boundary element method for the solution of the backward heat conduction equation. *J. Comp. Phys.*, vol. 116, pp. 292-299.

Iijima, K. (2004): Numerical solution of backward heat conduction problems by a high order lattice-free finite difference method. *J. Chinese Inst. Engineers*, vol. 27, pp. 611-620.

Jourhmane, M.; Mera, N. S. (2002): An iterative algorithm for the backward heat conduction problem based on variable relaxation factors. *Inv. Prob. Eng.*, vol. 10, pp. 293-308.

Kirkup, S. M.; Wadsworth, M. (2002): Solution of in-

verse diffusion problems by operator-splitting methods. *Appl. Math. Model.*, vol. 26, pp. 1003-1018.

Lesnic, D.; Elliott, L.; Ingham, D. B. (1998): An iterative boundary element method for solving the backward heat conduction problem using an elliptic approximation. *Inv. Prob. Eng.*, vol. 6, pp. 255-279.

Liu, C.-S. (2001): Cone of non-linear dynamical system and group preserving schemes. *Int. J. Non-Linear Mech.*, vol. 36, pp. 1047-1068.

Liu, C.-S. (2004): Group preserving scheme for backward heat conduction problems. *Int. J. Heat Mass. Transf.*, vol. 47, pp. 2567-2576.

Liu, C.-S. (2005a): Nonstandard group-preserving schemes for very stiff ordinary differential equations. *CMES: Computer Modeling in Engineering & Sciences*, vol. 9, pp. 255-272.

Liu, C.-S. (2005b): Preserving constraints of differential equations by numerical methods based on integrating factors. *CMES: Computer Modeling in Engineering & Sciences*, in press.

Liu, J. (2002): Numerical solution of forward and backward problem for 2-D heat conduction equation. *J. Comp. Appl. Math.*, vol. 145, pp. 459-482.

Marsden, J. E.; Ratiu, T. S. (1994): *Introduction to Mechanics and Symmetry*. Springer-Verlag, New York.

Mera, N. S. (2005): The method of fundamental solutions for the backward heat conduction problem. *Inv. Prob. Sci. Eng.*, vol. 13, pp. 65-78.

Mera, N. S.; Elliott, L.; Ingham, D. B.; Lesnic, D. (2001): An iterative boundary element method for solving the one-dimensional backward heat conduction problem. *Int. J. Heat Mass Transf.*, vol. 44, pp. 1937-1946.

Mera, N. S.; Elliott, L.; Ingham, D. B. (2002): An inversion method with decreasing regularization for the backward heat conduction problem. *Num. Heat Transfer B*, vol. 42, pp. 215-230.

Muniz, W. B.; de Campos Velho, H. F.; Ramos, F. M. (1999): A comparison of some inverse methods for estimating the initial condition of the heat equation. *J. Comp. Appl. Math.*, vol. 103, pp. 145-163.

Muniz, W. B.; Ramos, F. M.; de Campos Velho, H. F. (2000): Entropy- and Tikhonov-based regularization techniques applied to the backward heat equation. *Int. J. Comp. Math.*, vol. 40, pp. 1071-1084.

Appendix A:

In this appendix we derive Eqs. (33) and (36) by another method. For the backward problem (24) we usually search a backward scheme, such that Eq. (13) is rewritten as

$$\mathbf{X}_\ell = \mathbf{G}(\ell)\mathbf{X}_{\ell-1}, \tag{A.1}$$

that is, we use the state at the ℓ-th step to calculate $\mathbf{G}(\ell)$, instead of the state at the $\ell-1$-th step to calculate $\mathbf{G}(\ell-1)$.

Taking the inverse of Eq. (A.1) we get a backward scheme:

$$\mathbf{X}_{\ell-1} = \mathbf{G}^{-1}(\ell)\mathbf{X}_\ell. \tag{A.2}$$

By using the group property (9) we have

$$\mathbf{G}^{-1}(\ell) = \mathbf{g}\mathbf{G}^T(\ell)\mathbf{g}. \tag{A.3}$$

Inserting Eq. (4) for $\mathbf{g}$ and Eq. (16) for $\mathbf{G}(\ell)$ into the above equation we obtain

$$\mathbf{G}^{-1}(\ell) = \begin{bmatrix} \mathbf{I}_n + \frac{2\tau^2}{\|\mathbf{x}_\ell\|^2-\tau^2\|\mathbf{f}_\ell\|^2}\mathbf{f}_\ell\mathbf{f}_\ell^T & -\frac{2\tau\|\mathbf{x}_\ell\|}{\|\mathbf{x}_\ell\|^2-\tau^2\|\mathbf{f}_\ell\|^2}\mathbf{f}_\ell \\ -\frac{2\tau\|\mathbf{x}_\ell\|}{\|\mathbf{x}_\ell\|^2-\tau^2\|\mathbf{f}_\ell\|^2}\mathbf{f}_\ell^T & \frac{\|\mathbf{x}_\ell\|^2+\tau^2\|\mathbf{f}_\ell\|^2}{\|\mathbf{x}_\ell\|^2-\tau^2\|\mathbf{f}_\ell\|^2} \end{bmatrix}. \tag{A.4}$$

Substituting Eq. (A.4) into Eq. (A.2) and taking the first row we obtain the numerical scheme in Eq. (33).

Similarly, inserting Eq. (4) for $\mathbf{g}$ and Eq. (19) for $\mathbf{G}(\ell)$ into Eq. (A.3) we obtain

$$\mathbf{G}^{-1}(\ell) = \begin{bmatrix} \mathbf{I}_n + \frac{(a_\ell-1)}{\|\mathbf{f}_\ell\|^2}\mathbf{f}_\ell\mathbf{f}_\ell^T & -\frac{b_\ell\mathbf{f}_\ell}{\|\mathbf{f}_\ell\|} \\ -\frac{b_\ell\mathbf{f}_\ell^T}{\|\mathbf{f}_\ell\|} & a_\ell \end{bmatrix}. \tag{A.5}$$

Substituting Eq. (A.5) into Eq. (A.2) and taking the first row we obtain the numerical scheme in Eq. (36).